Influences of different orbit interpolation methods on substitution accuracy of rational polynomial coefficient model for multi-mode images from Gaofen-3 Satellite

Liu Xin [1, 3], Deng Mingjun [1, 3, *], Yang Yin [2, 3], Zhou Yan [1, 3], Zhang Zhengpeng [1, 3]

[1] School of Automation and Electronic Information, Xiangtan University, Xiangtan 411105, China
[2] School of Mathematics and Computational Science, Xiangtan University, Xiangtan 411105, China
[3]National Center for Applied Mathematics in Hunan, Xiangtan 411105, Hunan, China

(Received Month Day, Year; accepted Month Day, Year; online published Month Day, Year)

Keywords: Orbit interpolation, geometric positioning, GF-3 satellite, RPC model, SAR image

Determining the satellite orbit vector is necessary when constructing the geometric positioning model for a Synthetic Aperture Radar image from the Gaofen-3 satellite (GF-3), as it greatly impacts the geometric positioning accuracy. Therefore, it is vital to obtain accurate orbit vector data regarding the satellite imaging time. Here, GF-3's orbit was interpolated using the Lagrange interpolation, Chebyshev polynomial, and ordinary polynomial methods, with each method's influence on the substitution accuracy of the Rational Polynomial Coefficient (RPC) model being analyzed for GF-3's various imaging modes. The results show that based on Lagrange interpolation orbit, the accuracy of RPC substitution is greatly affected by the length of the orbit, and the stability of RPC substitution accuracy is limited by the position of the interpolation orbit segment. In general, this method shows low RPC substitution accuracy and large fluctuations. The Chebyshev polynomial method and the ordinary polynomial method are less affected by the orbital length and can obtain high substitution accuracy. The RPC substitution accuracy of the two methods was higher than 0.08 % and 0.02 %, respectively. In addition, the results of RPC substitution accuracy are more stable and reliable when ordinary polynomial interpolation orbit is used.

1. Introduction

Launched in August 2016, the Gaofen-3 (GF-3) satellite has the most imaging modes of all Synthetic Aperture Radar (SAR) satellites. In detail, it possesses 12 imaging modes, such as traditional strip, scanning, and wave imaging modes, with an image resolution of 1–500 m and a width range of 10–650 km[1-3]. GF-3 is the first C-band multi-polarization SAR satellite with a resolution of 1 m from China[4]; it can continuously monitor and survey global marine and land resources in all-day and all-weather conditions, and provides strong suppor t for applications such as marine environment monitoring, marine target surveillance, sea area use management, marine

*Corresponding author: Deng Mingjun, e-mail: xtudmj@xtu.edu.cn

rights maintenance, and disaster prevention and mitigation. It can effectively change the status quo of relying on imported high-resolution SAR images in China, which is of great significance to maritime development and the success of the "One Belt, One Road" initiative[4-6].

With the rapid development of spaceborne SAR technology, SAR image positioning technology has increased in maturity. To date, several geometric models for spaceborne SAR positioning have been developed, with the main two being the Range-Doppler (RD) [7] and Rational Polynomial Coefficient (RPC) models[8]. The RD model is a geometric imaging model with a strict physical meaning; it consists of the slant range, Doppler, and ellipsoidal equations. This set of equations is constructed depending on the parameters of the sensor, and this model has a high threshold for use[9,10]. The RPC model, meanwhile, is a geometric imaging model with mathematical significance; it has strong versatility, and so could be used as a substitute for the RD model. As such, this model has been studied extensively, both in China and internationally. Toutin summarized the RD and RPC models in detail, revealing them to be the leading geometric imaging models[11], while Tao *et al.* studied the forms of the positive and negative mathematics of the RPC model in depth and analyzed the influence of the control point distribution on its fitting accuracy[12,13]. Zhang *et al.*, meanwhile, verified the feasibility and effectiveness of substituting the RD model with the RPC model, based on SAR image product data[14,15]. Hou et al. analyzed the factors influencing the fitting accuracy of the RPC model based on GF-3's image products, mainly including the grid size, elevation layers, and fitting order[16]. The orbit data represent an important element when constructing spaceborne SAR tight geometric positioning models, so their accuracy can significantly influence the substitution accuracy of the RPC model. At present, however, the orbit lengths available for interpolation differ across GF-3's diverse imaging modes. Moreover, to date the effect of using different orbit interpolation methods has not been investigated regarding the substitution accuracy of the RPC model for GF-3 images.

The commonly used interpolation methods for satellite orbits are Lagrange interpolation, the Chebyshev polynomial method, and the ordinary polynomial method[17,18]. These methods are based on the position and velocity of a given satellite, and corresponding mathematical models are constructed for interpolation to obtain said satellite's orbit state corresponding to the imaging time of each image line. There are large differences in imaging time between each of GF-3's imaging modes (Table 1), with longer imaging times resulting in a greater degree of orbit bending. Thus, it is important to investigate the mathematical modeling of the orbital parameters of GF-3 using different interpolation methods, and to analyze the influence of each interpolation method on the RPC model's substitution accuracy under different imaging modes.

Table 1 GF-3 imaging mode.

Imaging mode	Resolution (m)	Image ID	Imaging time (s)
Ultra-Fine-Strip	3	HZ_1202	5.5
		HW_3468	5.0
Fine-Strip-I	5	BF_5833	9.0
		SP_2388	9.0
Quad-Polarized-Strip-I	8	SP_2272	5.1
		BF_9197	6.0

This study analyzed the establishment of the RPC positioning model and the parameter solving process. Furthermore, based on the RPC model substitution accuracies of different GF-3 product

images, the effects of three orbit interpolation algorithms (Lagrange interpolation, the Chebyshev polynomial method, and the ordinary polynomial method) were analyzed and verified.

2. Methods

2.1 RPC model

The RPC model correlates the relationship between the coordinates of ground target points and the coordinates of points on corresponding images using a ratio polynomial; it is defined as shown in Equation (1) [19]:

$$\begin{cases} Y = \dfrac{N_L(P,L,H)}{D_L(P,L,H)} \\ X = \dfrac{N_S(P,L,H)}{D_S(P,L,H)} \end{cases}, \tag{1}$$

where $N_L(P,L,H)$, $D_L(P,L,H)$, $N_S(P,L,H)$, and $D_S(P,L,H)$ are third-order polynomials, with each polynomial having 20 coefficients; the constant parameter of the general denominator was set here to 1, leading to the RPC model having 78 parameters in total. Furthermore, (X,Y) denotes the regularized image space coordinates, while (P,L,H) represents the regularized ground space coordinates. The regularization formula is shown in Equations (2), (3):

$$\begin{cases} X = \dfrac{S - S_{off}}{S_{scale}} \\ Y = \dfrac{L - L_{off}}{L_{scale}} \end{cases}, \tag{2}$$

$$\begin{cases} P = \dfrac{D_{lat} - D_{lat\_off}}{D_{lat\_scale}} \\ L = \dfrac{D_{lon} - D_{lon\_off}}{D_{lon\_scale}} \\ H = \dfrac{D_h - D_{h\_off}}{D_{h\_scale}} \end{cases}, \tag{3}$$

where S_{off}, S_{scale}, L_{off}, and L_{scale} are the normalized parameters of the coordinates of the corresponding points on the image, while D_{lat}, D_{lat_off}, D_{lat_scale}, D_{lon}, D_{lon_off}, D_{lon_scale}, D_h, D_{h_off}, and D_{h_scale} are the normalized parameters of the coordinates of the ground target points. Many studies have shown that the RPC model exhibits the highest replacement accuracy when used with third order and unequal denominators. The following experiments were therefore

conducted based on this model; the grid size was set to 200 × 200 and the number of elevation layers was 15[16,20].

2.2 Orbit interpolation method

In the azimuthal direction, each line of the GF-3 image corresponds to the position and velocity of a satellite and is a function of time (t). It can be interpolated by Lagrange interpolation[21], the Chebyshev polynomial method[22], or the ordinary polynomial method to obtain the orbit vector and the function of t.

2.2.1 Lagrange interpolation method

The Lagrange interpolation method is widely used due to its simplicity and computation speed. The Lagrange interpolation function is defined as shown in Equation (4)[23]:

$$L(x)=\sum_{j=0}^{k} y_j l_j(x), \tag{4}$$

where $l_j(x)$ is the Lagrange interpolation basis function, the expression of which is given by Equation (5):

$$\begin{aligned} l_j(x) &= \prod_{i=0, i\neq j}^{k} \frac{x-x_i}{x_j-x_i} \\ &= \frac{(x-x_0)}{(x_j-x_0)}\cdots\frac{(x-x_{j-1})}{(x_j-x_{j-1})}\frac{(x-x_{j+1})}{(x_j-x_{j+1})}\cdots\frac{(x-x_k)}{(x_j-x_k)} \end{aligned}, \tag{5}$$

and satisfies:

$$l_j(x_j)=\delta_{i,j}=\begin{cases}1, i=j\\ 0, i\neq j\end{cases}, (j=0,1,\cdots,k). \tag{6}$$

Assuming a k-order interpolation, there are k + 1 known points, and interpolation can be carried out at any position between these k + 1 points. Thus, the position coordinates and velocity of GF-3 can be calculated as shown in Equation (7) using the WGS-84 coordinate system:

$$\begin{cases} x(t)=\sum_{j=0}^{k} l_j f(x_j) \\ y(t)=\sum_{j=0}^{k} l_j f(y_j) \\ z(t)=\sum_{j=0}^{k} l_j f(z_j) \\ x_v(t)=\sum_{j=0}^{k} l_j f(x_{vj}) \\ y_v(t)=\sum_{j=0}^{k} l_j f(y_{vj}) \\ z_v(t)=\sum_{j=0}^{k} l_j f(z_{vj}) \end{cases}. \tag{7}$$

2.2.2 Chebyshev polynomial method

The Chebyshev polynomial method, which generates interpolated polynomial coefficients based on known nodes and relies on least-squares approximation, has important applications regarding approximation theory. When computing the Chebyshev polynomial coefficients of order k for a time interval of $\Delta t=\left[t_0,t_0+d_t\right]$ (where t_0 = initial time and d_t = interpolation time length), the Chebyshev polynomial can be defined as shown in Equation (8) [24]:

$$f(t)=\sum_{i=0}^{k} C_i T_i(\tau), \tag{8}$$

where $\tau\in\left[-1,1\right]$ is transformed from the time interval, k denotes the order, C_i is the Chebyshev polynomial coefficient, and T_i is the Chebyshev polynomial. T_i can be obtained recursively, as shown in Equation (9):

$$\begin{cases} T_0(\tau)=1 \\ T_1(\tau)=\tau \\ T_{k+1}(\tau)=2\tau T_k(\tau)-T_{k-1}(\tau) \end{cases} ,|\tau|\le 1, k\ge 2. \tag{9}$$

Thus, the coordinates of a satellite in the WGS-84 coordinate system, as well as its velocity, can be interpolated using the Chebyshev polynomial function, as shown in Equation (10):

$$\begin{cases} x(t)=\sum_{i=0}^{k} C_{xi}T_i(\tau) \\ y(t)=\sum_{i=0}^{k} C_{yi}T_i(\tau) \\ z(t)=\sum_{i=0}^{k} C_{zi}T_i(\tau) \\ x_v(t)=\sum_{i=0}^{k} C_{xvi}T_i(\tau) \\ y_v(t)=\sum_{i=0}^{k} C_{yvi}T_i(\tau) \\ z_v(t)=\sum_{i=0}^{k} C_{zvi}T_i(\tau) \end{cases}. \tag{10}$$

If the error equation is $\boldsymbol{V}=\boldsymbol{BC}-\boldsymbol{F}$, then, taking the x coordinate as an example[25]:

$$\boldsymbol{B}=\begin{bmatrix} T_0(\tau_1) & T_1(\tau_1) & \cdots & T_n(\tau_1) \\ T_0(\tau_2) & T_1(\tau_2) & \cdots & T_n(\tau_2) \\ \vdots & \vdots & \vdots & \vdots \\ T_0(\tau_m) & T_1(\tau_m) & \cdots & T_n(\tau_m) \end{bmatrix}, \tag{11}$$

$$\begin{cases} \boldsymbol{V}=\begin{vmatrix} V_{x1} & V_{x2} & V_{x3} & \cdots & V_{xm} \end{vmatrix}^T \\ \boldsymbol{C}=\begin{vmatrix} C_{x1} & C_{x2} & C_{x3} & \cdots & C_{xm} \end{vmatrix}^T \\ \boldsymbol{F}=\begin{vmatrix} X_{x1} & X_{x2} & X_{x3} & \cdots & X_{xm} \end{vmatrix}^T \end{cases}. \tag{12}$$

2.2.3 Ordinary polynomial method

The N[th] order ordinary polynomial is expressed as shown in Equation (13)[18]:

$$y=P(x)=a_n x^n+a_{n-1}x^{n-1}+\cdots+a_1 x+a_0, \tag{13}$$

where $a_1, a_1, \cdots a_n$ is a polynomial coefficient, $P(x)$ represents a satellite's coordinates (x, y, z) and velocity (x_v, y_v, z_v) at the point target imaging time x, and x is the time interval from the moment in question to the starting point of the interpolation period.

Therefore, when calculating the position of a given satellite at any moment, the time function of its coordinates and velocity can be constructed from the expression of the ordinary polynomial, as shown in Equation (14):

$$\begin{cases} x(t) = a_{xn}t^n + a_{x(n-1)}t^{n-1} + \cdots + a_{x1}t + a_{x0} \\ y(t) = a_{yn}t^n + a_{y(n-1)}t^{n-1} + \cdots + a_{y1}t + a_{y0} \\ z(t) = a_{zn}t^n + a_{z(n-1)}t^{n-1} + \cdots + a_{z1}t + a_{z0} \\ x_v(t) = a_{xvn}t^n + a_{xv(n-1)}t^{n-1} + \cdots + a_{xv1}t + a_{xv0} \\ y_v(t) = a_{yvn}t^n + a_{yv(n-1)}t^{n-1} + \cdots + a_{yv1}t + a_{yv0} \\ z_v(t) = a_{zvn}t^n + a_{zv(n-1)}t^{n-1} + \cdots + a_{zv1}t + a_{zv0} \end{cases}. \quad (14)$$

3. Experimental Method

3.1 Experimental data

In this study, GF-3 SAR images were used as experimental data. To compare the effects of different orbit interpolation methods on the RPC model's substitution accuracy under different imaging modes, the Ultra-Fine-Strip (UFS), Fine-Strip-I (FSI), and Quad-Polarized-Strip-I (QPSI) image modes were analyzed; these modes cover the Zhengzhou (Henan), Pudong (Shanghai), Fangshan (Beijing), and Wenchang (Hainan) areas, which were selected for testing. More detailed information about these three test modes is listed in Table 2.

Table 2 Test image parameters.

Imaging Mode	Image ID	Region	Orbit & Side View	Angle of Incidence (°)	Imaging Start Time	Imaging End Time	Imaging Time (s)	Number of GPS Track Vectors Recorded in Imaging Information Parameter File (unit)
Ultra-Fine-Strip	HZ_1202	Henan	DEC&R	33.5	2019/10/21 22:30:56	2019/10/21 22:31:01	5.5	361
	HW_3468	Hainan	ASC & R	28.4	2020/4/21 10:44:19	2020/4/21 10:44:24	5.0	301
Fine-Strip-I	BF_5833	Beijing	ASC & R	30.7	2017/10/19 10:09:52	2017/10/19 10:10:01	9.0	234
	SP_2388	Shanghai	ASC & R	20.2	2019/12/26 9:48:48	2019/12/26 9:48:57	9.0	361
Quad-Polarized-Strip-I	BF_9197	Beijing	ASC & R	18.9	2017/1/22 21:51:22	2017/1/22 21:51:27	5.0	241
	SP_2272	Shanghai	DEC&R	31.7	2017/05/30 21:55:07	2017/05/30 21:55:13	5.1	212

GPS: Global Positioning System; ASC: Ascending Orbit; DEC: Descending Orbit; R: Right Side View

3.2 Experimental program

An experiment was designed to compare and verify the effects of the three interpolation methods on the RPC model's substitution accuracy when using GF-3's different imaging modes. The experiment was based on different lengths of track segments from a single image for each mode. GF-3's satellite image imaging information parameter file records a satellite position vector every 1 s, so the track segments were divided into track lengths composed of the GPS orbit vector recorded by the imaging information parameter file (hereinafter referred to as track 1) and the length of the track at the imaging moment of a single SAR standard view image (hereinafter referred to as track 2; Fig. 1).

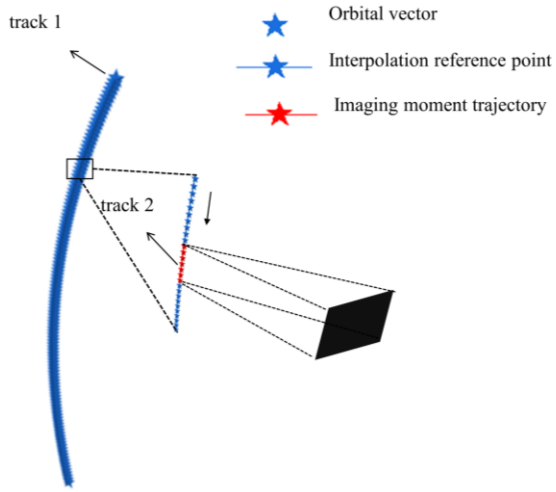

Fig. 1 Imaging trajectory diagram of a GF-3 SAR image.

The experiment was set on the basis of the length of track 2. The number of track vectors was then gradually increased, that is, the time difference of Coordinated Universal Time (UTC) corresponding to the positions of the interpolation start and end nodes was increased accordingly to characterize the acquisition of different orbit lengths. The UFS, FSI, and QPSI modes are 10 s apart. Based on the above experimental design, the orbit vectors of the different imaging mode images were interpolated with each of the three abovementioned interpolation methods to obtain the satellite vectors at arbitrary positions. Then, the RD model was fitted with the RPC model, with the Root Mean Square Error (RMSE) being used as an evaluation index to evaluate the substitution accuracy obtained by the RPC model under the three methods.

4. Experimental results and analysis

4.1 Effect of Lagrange interpolation-based method on RPC model substitution accuracy for different imaging modes

Figure 2 shows the fitting results for each of the three test pattern images; the statistical RPC substitution accuracy results are shown in Table 3.

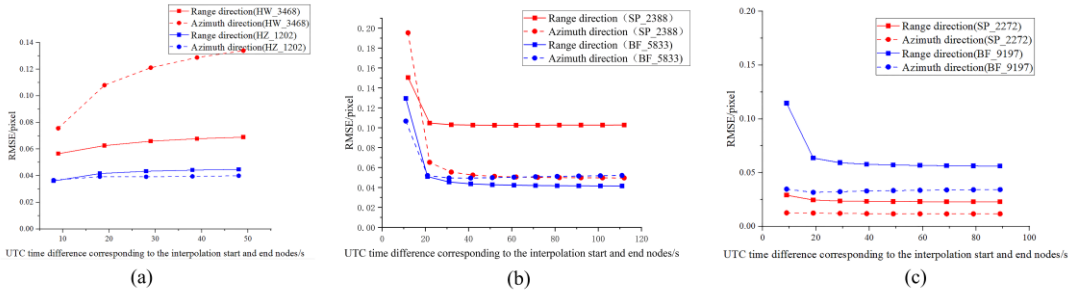

Fig. 2 Rational Polynomial Coefficient substitution accuracy based on Lagrange interpolation:

(a) Ultra-Fine-Strip mode image, (b) Fine-Strip-I mode image, and (c) Quad-Polarized-Strip-I mode image.

Figure 2 (a) shows that the RPC substitution error of the UFS mode image was proportional to the UTC time difference corresponding to the interpolation starting and ending nodes. As the length of the UTC time difference between the two images of the UFS mode in the figure is limited, using more track vectors for interpolation would have made it easier to approach the end point of Track 1. Lagrange interpolation is prone to Runge's phenomenon at the end point, so it is reasonable that the error of this test result increased approaching the end point. Figure 2 (b, c) shows that the RPC substitution errors of each scene image decreased with increasing UTC time difference corresponding to the interpolation start and end nodes. This trend occurred because the arc of the track segment corresponding to the starting and ending nodes of the interpolation is large. The larger the time difference is, the longer the track length formed by the track vector. Therefore, the RPC substitution accuracy is better after Lagrange interpolation. This indicates that when using Lagrange interpolation, it is difficult to avoid Runge's phenomenon due to the irregular position of the interpolation point. Therefore, the RPC substitution accuracy after interpolation was neither good nor bad, indicating that using this method for interpolation results in an unreliable RPC substitution accuracy.

Table 3 Substitution accuracy analysis of Rational Polynomial Coefficient model based on Lagrange interpolation.

Imaging Mode	Imaging ID	RMSE (pixel)	
		Range Direction	Azimuth Direction
Ultra-Fine-Strip	HZ_1202	0.03606	0.03671
	HW_3468	0.05653	0.07562
Fine-Strip-I	BF_5833	0.12945	0.10659
	SP_2388	0.15042	0.19535
Quad-Polarized-Strip-I	BF_9197	0.11449	0.03473
	SP_2272	0.02901	0.01262

Table 3 shows that the imaging time of the FSI mode image is the longest, and the length of the corresponding track 2 is the longest. Its RPC has the worst substitution accuracy in the range and azimuth directions, and the worst substitution accuracy is 15.042% and 19.535% pixels. Even

though the RPC substitution accuracy of UFS and QPSI images is relatively good, it is only within 9% pixels, meaning that it will be difficult for it to meet the needs of GF-3 applications.

4.2 Effect of Chebyshev polynomial-based method on RPC model substitution accuracy for different imaging modes

Figure 3 shows the error statistics for the RPC model's substitution accuracy regarding the three experimental model images (Table 4).

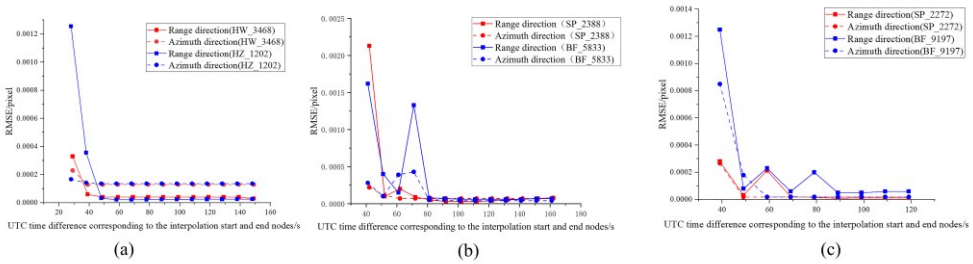

Fig. 3 Rational Polynomial Coefficient substitution accuracy based on Chebyshev polynomial:

(a) Ultra-Fine-Strip mode image, (b) Fine-Strip-I mode image, and (c) Quad-Polarized-Strip-I mode image.

In theory, for Chebyshev polynomial interpolation, using more points for interpolation should help to improve the accuracy of polynomial interpolation. Figure 3 shows that the larger the UTC time difference corresponding to the interpolation start and end nodes (i.e., the longer the track length composed of the track vector), the smaller the RPC substitution error was for each mode's image. This indicates that using longer track segments for interpolation delivered a better RPC substitution accuracy when using the Chebyshev polynomial interpolation track.

Table 4 Substitution accuracy analysis of Rational Polynomial Coefficient model based on Chebyshev polynomial method.

Imaging Mode	Imaging ID	RMSE (pixel)	
		Range Direction	Azimuth Direction
Ultra-Fine-Strip	HZ_1202	0.000017	0.000136
	HW_3468	0.00002	0.00013
Fine-Strip-I	BF_5833	0.00009	0.00004
	SP_2388	0.00078	0.00007
Quad-Polarized-Strip-I	BF_9197	0.00015	0.00002
	SP_2272	0.00001	0.00002

Table 4 shows that the RPC replacement accuracy of the above image products was within 0.08% pixels for the range and azimuth directions when using the Chebyshev polynomial interpolation orbit; this would meet GF-3's operational requirements. Compared with Table 3, the substitution accuracy of RPC was significantly improved. Considering that Chebyshev polynomial interpolation can more effectively avoid Runge's phenomenon, the substitution

accuracy of the RPC was more accurate after interpolation by this method, indicating that the test results were reasonable.

4.3 Effect of ordinary polynomial-based method on RPC model substitution accuracy for different imaging modes

Figure 4 shows the distribution of RPC substitution errors based on ordinary polynomial interpolation for tests conducted with three test pattern images; the RPC model substitution accuracy is shown in Table 5.

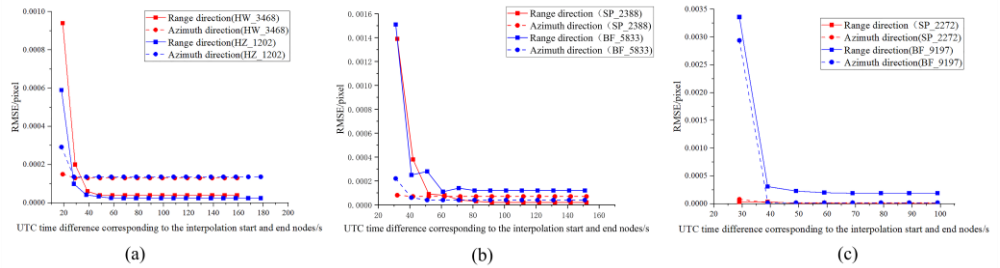

Fig. 4 Rational Polynomial Coefficient substitution accuracy error based on ordinary polynomial:

(a) Ultra-Fine-Strip mode image, (b) Fine-Strip-I mode image, and (c) Quad-Polarized-Strip-I mode image.

The accuracy of ordinary polynomial interpolation is affected by the number of interpolation points; using more interpolation nodes results in an improved accuracy. Figure 4 shows that, for all three images, as the number of nodes used for interpolation increased with increasing track length (and correspondingly increasing UTC duration), the substitution accuracy of the RPC model gradually decreased, before stabilizing when using the ordinary polynomial interpolation track.

Table 5 Substitution accuracy analysis of Rational Polynomial Coefficient model based on ordinary polynomial method.

Imaging Mode	Imaging ID	RMSE (pixel)	
		Range Direction	Azimuth Direction
Ultra-Fine-Strip	HZ_1202	0.00002	0.00014
	HW_3468	0.00004	0.00013
Fine-Strip-I	BF_5833	0.00012	0.00004
	SP_2388	0.00002	0.00007
Quad-Polarized-Strip-I	BF_9197	0.00019	0.00002
	SP_2272	0.00001	0.00002

The results in Table 5 show that the RPC model obtained good substitution accuracy when using the ordinary polynomial method interpolated orbit, and that the substitution accuracy reached within 0.02% pixels for each mode's image under different orbit lengths. This indicates

that the ordinary polynomial method interpolation orbit can obtain more accurate orbit data than Lagrange interpolation, and that the RPC model's substitution accuracy was reliable.

5. Conclusions

This study investigated the influence of using different orbit interpolation methods on the replacement accuracy of the RPC model for several of GF-3's image modes. This was experimentally investigated using the imaging information file data of GF-3's SAR images. The specific conclusions are as follows:

1. The replacement accuracy of the RPC model was found to be related to the orbit interpolation method. Among them, the Lagrange interpolation method effect < Chebyshev polynomial interpolation effect < polynomial interpolation effect. When the polynomial interpolation method is used, the substitute accuracy of RPC is <0.02% pixels.

2. For the GF-3 satellite images, the results obtained by the Lagrange interpolation method are greatly affected by the interpolation orbit length. The imaging time of the FSI mode is longer than that of the other two modes, and the substitution accuracy of RPC in the FSI mode is one order of magnitude lower than that of the other two modes. The results of Chebyshev polynomial interpolation and ordinary polynomial interpolation are less affected by the length of the interpolation orbit, and the RPC substitution accuracy of the two methods is better than 0.08 % and 0.02 %, respectively. In addition, polynomial interpolation is more stable than Chebyshev polynomial interpolation.

The results presented here show using the ordinary polynomial method to interpolate the orbit delivered more accurate, stable, and reliable results than those of the other two methods. This study's findings could provide reference values for subsequent experimental positioning calibration studies. They could also aid other experimental studies into the selection of geometric imaging positioning models under different scenarios.

Acknowledgments

This study was supported by the Key Research and Development Program of China (No.2020YFA0713503) and the Nature Science Foundation of Hunan Province (Grant No. 2020JJ5537).

References

1 J. Sun, W. Yu, and Y. Deng, "The SAR payload design and performance for the GF-3 mission," Sensors 17(10), 2419 (2017) [doi:10.3390/s17102419].

2 T. Wang et al., "Multi-mode GF-3 satellite image geometric accuracy verification using the RPC model," *Sensors* **17**(9), 2005 (2017) [doi:10.3390/s17092005].

3 D. Pang, C. Pan, and X. Zi, "GF-3: The watcher of the vast territory," *Aerosp. China* **9**, 8-12 (2016).

4 R. Zhao et al., "Geometric calibration and accuracy verification of the GF-3 satellite," *Sensors* **17**(9), 1977 (2017) [doi:10.3390/s17091977].

5 M. Deng, G. Zhang, R. Zhao, S. Li, and J. Li, "Improvement of Gaofen-3 Absolute Positioning Accuracy Based on Cross-Calibration," *Sensors* **17**(12), 2903 (2017) [doi:10.3390/s17122903].

6 Z. Qingjun, "System design and key technologies of the GF-3 satellite," *Acta Geodaetica et Cartographica Sinica* **46**(3), 269 (2017) [doi:10.11947/j.AGCS.2017.20170049].

7 J. C. Curlander, "Location of spaceborne SAR imagery." *IEEE Transactions on Geoscience and Remote Sensing* **3**, 359-364 (1982) [doi: 10.1109/TGRS.1982.350455].

8 J. Grodecki, and G. Dial, "Block adjustment of high-resolution satellite images described by rational polynomials," *Photogramm. Eng. Remote Sens*. **69**, 59–68 (2003) [doi:10.14358/PERS.69.1.59].

9 J. C. Curlander, and R. N. McDonough, *Synthetic Aperture Radar Systems and Signal Processing*, Hoboken, NJ, USA, Wiley (1991).

10 X. Wei, B. Jin, G. Jiao, C. Xi, and W. Zheng, "Geolocation analysis for near-space synthetic aperture radar based on Rang-Doppler model," *2021 2nd China International SAR Symposium (CISS)*, 1-5 (2021) [doi:1s0.23919/CISS51089.2021.9652232].

11 T. Toutin, "Geometric processing of remote sensing images: models, algorithms and methods," *International journal of remote sensing* **25**(10), 1893-1924 (2004) [doi:10.1080/0143116031000101611].

12 C. V. Tao, and Y. Hu, "Investigation of the rational function model," *Proceedings of 2000 ASPRS Annual Convention*, (2000).

13 C.V. Tao, "Image rectification using a generic sensor model-rational function model," *International Archives of Photogrammetry and Remote Sensing*, B **33**(3), 874-881 (2000).

14 G. Zhang, et al., "Evaluation of the RPC model for spaceborne SAR imagery," *Photogrammetric Engineering & Remote Sensing* **76**(6), 727-733 (2010) [doi:10.14358/PERS.76.6.727].

15 G. Zhang, W. B. Fei, Z. Li, X. Zhu, and X. Tang. "Analysis and test of the substitutability of the RPC model for the rigorous sensor model of spaceborne SAR imagery," *Acta Geodaetica et Cartographica Sinica* **39**(3), 264-270 (2010).

16 S. Hou, et al., "Feasibility of Replacing the Range Doppler Equation of Spaceborne Synthetic Aperture Radar Considering Atmospheric Propagation Delay with a Rational Polynomial Coefficient Model," *Sensors (Basel, Switzerland)* **20**(2), 553 (2020) [doi:10.3390/s20020553].

17 J-. Y. Richard, F. Deleflie, and D. Gambis, "Satellite Orbital Interpolation Comparison Methods," *EGU General Assembly Conference Abstracts*, 8259 (2012).

18 M. Horemuž, and J. V. Andersson, "Polynomial interpolation of GPS satellite coordinates," *GPS Solutions* **10**(1), 67-72 (2006) [doi:10.1007/s10291-005-0018-0].

19 K. S. S. Sekhar, A. Senthil Kumar, and V. K. Dadhwal, "Geocoding RISAT-1 MRS images using bias-compensated RPC models." *International Journal of Remote Sensing* **35**(20) 7303-7315 (2014) [doi:10.1080/01431161.2014.968266].

20 N. G. Jiao, F. Wang, H. J. You, X. L. Qiu, and M. D. Yang, "Geo-positioning accuracy improvement of multi-mode gf-3 satellite SAR imagery based on error sources analysis," *Sensors* **18**, 2333 (2018) [doi:10.3390/s18072333].

21 L. Fokin, A. Shchipitsyn, and Y. Shtessel, "Adaptive SINS/ANS/GNSS for air-launch space launcher: Algorithm design and performance analysis," *AIAA Guidance, Navigation, and Control Conference* **4**, 3995-4013 (2007) [doi:10.2514/6.2007-6760].

22 Z. Sun, and S. Li, "Method of solving optimal inventory control with Chebshev approximation," *Kongzhi yu Juece/Control and Decision* **24**(5) 767-800 (2009).

23 H. Hu, and L. Fang, "Interpolation and fitting algorithms for GPS satellite orbit," *2009 International Conference on Photonics and Image in Agriculture Engineering, PIAGENG 2009, Proc. of SPIE* **7491**(749109), 1-5 (2009) [doi:10.1117/12.836851].

24 S. F. Xie, P. F. Zhang, and L. L. Liu, "Analyzing the precision of Chebyshev polynomial fitting GPS satellite ep hemeris," *Applied Mechanics and Materials* **353**, 3410-3413 (2013) [doi:10.4028/www.scientific.net/AMM.353-356.3410].

25 H. Hu, C. Yuan, and L. Fang, "Extrapolation and Fitting Algorithms for GLONASS Satellite Orbit," *2009 Third International Symposium on Intelligent Information Technology Application* **3**, 282-285 (2009) [doi:10.1109/IITA.2009.484].